To cite this article: QIU J T, YIN X H, WANG R Z. Hydrodynamic performance analysis of waterjet propulsor inlet duct [J/OL]. Chinese Journal of Ship Research, 2022, 17(1). http://www. ship-research. com/en/article/doi/10.19693/j.issn.1673-3185.02269.

DOI: 10.19693/j.issn.1673-3185. 02269

Hydrodynamic performance analysis of waterjet propulsor inlet duct

QIU Jitao[*1, 2], *YIN Xiaohui*[1, 2], *WANG Renzhi*[2]

1 Science and Technology of Water Jet Propulsion Laboratory, Shanghai 200011, China;
2 Marine Design and Research Institute of China, Shanghai 200011, China

Abstract: [**Objectives**] The effects of the key parameters of the inlet duct of a waterjet propulsor on its hydrodynamic performance are studied, providing references for the design of waterjet propulsors. [**Methods**] With the commercial software STAR-CCM+, the influence of the axis height and inlet angle of a waterjet inlet duct on its hydrodynamic performance under different inlet velocity ratio (IVR) conditions is studied through numerical simulation using the steady Reynolds-averaged Navier-Stokes (RANS) equations. Numerical uncertainty analysis is carried out according to the International Towing Tank Conference (ITTC) uncertainty analysis procedure. In this paper, the computational domain is discretized with hexahedral structured grids. The set of governing equations is closed using the Realizable k-ε two-layer turbulence model, and the discretization schemes are second-order accurate. The semi-implicit method for pressure-linked equations (SIMPLE) algorithm is applied in the pressure-velocity coupling calculation. [Results] The results show that the numerical uncertainty is less than 4%, indicating that the grids used in this paper yield well-converged and reliable numerical results. [**Conclusions**] The efficiency of the inlet duct is higher in the range of IVR=0.7−1.1. For a large IVR, the inlet angle should be reduced. For a small IVR, the axis height can be appropriately increased to improve the homogeneity of flow at the outlet of the inlet duct.

Key words: waterjet propulsor; inlet duct; numerical uncertainty; hydrodynamic performance

CLC number: U664.34; U661.1

0 Introduction

Waterjet propulsors are widely used in high-speed ships owing to their high efficiency and excellent anti-cavitation performance at high speeds. Such propulsors mainly have three flow passage components: inlet duct, waterjet pump, and nozzle. Specifically, the design of the inlet duct has an important influence on whether the waterjet propulsor can offer excellent performance. On the one hand, the uniformity of the flow field at the inlet of the pump directly affects the hydrodynamic performance and cavitation performance of the pump, while the configuration of the inlet duct determines the characteristics of this flow field. On the other hand, the design of the inlet duct also needs to take into account its adaptability to working conditions, and an unreasonable design increases flow passage loss, resulting in a decrease in the efficiency of the propulsor.

With the rapid development of computational fluid dynamics (CFD), CFD technology is increasingly widely used in the design, performance analysis, and other research of the inlet duct of waterjet propulsors [1-2]. Shi et al. [3] adopted the Reynolds-averaged Navier-Stokes (RANS) method and the shear-stress transport (SST) turbulence model to study the flow characteristics of the flow field in the inlet duct of duct models with different inlet lengths under different inlet velocity ratios. The results show that increasing the inlet length of the inlet duct to a proper extent can improve the flow performance of the inlet duct. Li et al. [4] employed the RANS method and the renormalization group (RNG) k-ε turbu-

Received: 2021 − 01 − 17 **Accepted**: 2021 − 05 − 24

Supported by: Key Laboratory Fund of Water Jet Propulsion Technology (6142223190106)

Authors: QIU Jitao, male, born in 1994, master's degree, assistant engineer
YIN Xiaohui, female, born in 1980, master's degree, professor
WANG Renzhi, male, born in 1996, master's degree, assistant engineer

***Corresponding author**: QIU Jitao

lence model to investigate the internal flow characteristics of duct models with different inlet angles. According to their calculation results, the characteristics of the flow field in the duct worsen as the duct's inclination angle increases under the simulated inlet velocity ratio. Ji et al. [5] studied the influences the lip shape of the inlet duct has on the outlet flow non-uniformity and the position of the stagnation point and obtained its influence laws. Their results can guide the design of the inlet duct lip. Yang et al. [6] analyzed the parameters of the inlet duct of the waterjet propulsor. The results demonstrate that the diameter of the inlet duct has large influences on the non-uniformity of the outlet flow field, blade cavitation, and nozzle velocity. The diameter of the inlet duct should be given due consideration in the optimization and improvement of the inlet duct to improve the duct's adaptability to working conditions. At present, studies reported on the hydrodynamic performance of the inlet duct of waterjet propulsors are limited, and most of them are CFD numerical studies. As for CFD numerical simulations, their reliability is particularly important, so analyzing the uncertainty of numerical simulation is necessary. In addition, as the key parameters affecting the hydrodynamic performance of the inlet duct are not unique, comprehensive multi-parameter research is required.

Engineering practice shows that the key geometric parameters affecting the performance of the inlet duct are the axis height and the inlet angle. Therefore, this study attempts to use the CFD technology to investigate the influences of the axis height and the inlet angle of the inlet duct on the non-uniformity of the outlet flow field under different inlet velocity ratios and the flow loss of the duct (flow loss is evaluated by duct efficiency). Then, numerical uncertainty is analyzed according to the uncertainty analysis procedure recommended by the International Towing Tank Conference (ITTC) [7-8].

1 Numerical simulation method for hydrodynamic performance of inlet duct

In this study, the RANS method is adopted to simulate the hydrodynamic performance of the inlet duct. The definition of the geometric parameters of the inlet duct and the computational domain model are shown in Fig. 1 and Fig. 2, respectively. In these figures, D is the outlet diameter of the inlet duct; H is the axis height, i.e. the distance from the outlet centerline (axis) to the bottom of the ship; α is the inlet angle, i.e., the angle between the inclined section of the inlet duct and the ship bottom. The inlet duct is 40D away from the upstream inlet and 20D away from the downstream outlet, and the calculational domain has a width of 10D and a depth of 8D. The upstream inlet is a velocity inlet, and the downstream outlet is a pressure outlet. The outlet of the inlet duct is a mass flow outlet, and the sides and the bottom of the computational domain are symmetric planes. The other boundaries are non-slip walls, and the reference pressure is atmospheric pressure. Numerical simulations of multiple working conditions are implemented by changing the flow Q at the outlet of the duct.

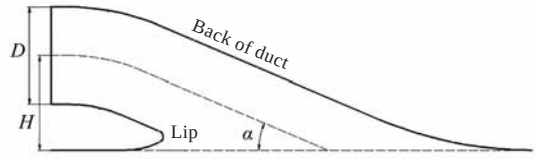

Fig. 1 Definition of geometric parameters of inlet duct

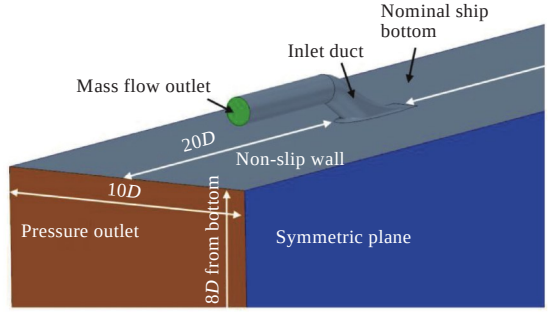

Fig. 2 Computational domain model

In this study, the commercial software STAR-CCM+ is used for steady RANS simulation, and the Realizable k-ε two-layer turbulence model is applied to close the governing equations. The full y^+ method is adopted to deal with the wall flow so that the solution can be adapted to situations of low Reynolds numbers ($y^+\approx1$) as well as those characterized by high Reynolds numbers ($y^+>30$) and thus requiring the employment of the wall function. Second-order accurate discretization schemes are adopted for the governing equations, and the semi-implicit method for pressure-linked equations (SIMPLE) algorithm is applied in the pressure-velocity coupling calculation.

The hydrodynamic performance parameters of the inlet duct are defined as follows: A control volume is selected to study the efficiency of the inlet duct and the outlet flow non-uniformity. The outlet

of the control volume is the actual outlet of the inlet duct, and its inlet is the semi-elliptic cross-section, also known as the capture area[9], 1*D* in front of the intersection of the front of the duct and the bottom of the ship. This cross-section is perpendicular to the axis, and its area can be determined according to the streamline under the corresponding working condition. Meanwhile, the inlet flow should be equal to the outlet flow, as shown in Fig. 3.

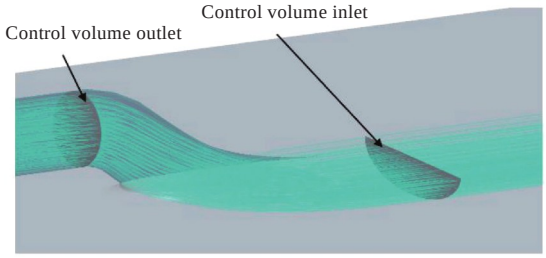

Fig. 3 Inlet and outlet of control volume

Inlet velocity ratio *IVR*, inlet duct efficiency η, and outlet flow non-uniformity ζ are defined as follows:

$$IVR = \frac{V_{\text{out}}}{V_{\text{in}}} \tag{1}$$

$$\eta = \frac{p_{\text{Tout}}}{p_{\text{Tin}}} \tag{2}$$

$$\zeta = \frac{1}{Q}\int |u - V_{\text{out}}| \mathrm{d}A \tag{3}$$

where V_{in} is the free inflow velocity, m/s; V_{out} is the average velocity at the outlet of the inlet duct, m/s. They are both axial velocities; p_{Tin} and p_{Tout} are the total pressure (excluding atmospheric pressure) at the inlet and actual outlet of the control volume, respectively, Pa; Q is the flow at the outlet, m^3/s; u is the axial velocity at the control volume outlet, m/s; dA is the outlet area microelement.

2 Uncertainty analysis

In this study, the outlet diameter D of the inlet duct is 200 mm. The working condition of H = 1.0D, α = 33°, *IVR* = 0.7 (free inflow velocity V_{in} = 10 m/s, the outlet flow Q of the inlet duct is 0.22 m^3/s) is selected to study the boundary rationality and uncertainty of the simulated η and ζ.

Hexahedral structured grids are used to discretize the computational domain, and the grid topology of the mid-longitudinal section is presented in Fig. 4. Three sets of grids (coarse, medium, and fine) are obtained through grid division by the same grid refinement ratio ($r_{\text{G}} = \sqrt{2}$) for uncertainty analysis. The key parameters of the three sets of grids are shown in Table 1.

(a) Coarse grids (b) Medium grids (c) Fine grids

Fig. 4 Grid topology of mid-longitudinal section

Table 1 Key parameters of grids

Grids	Grid size of inlet duct/mm	Grid height of the first layer of wall/mm	Total number of grids
Coarse grids	7.07	0.002 0	70×10^4
Medium grids	5.00	0.001 4	198×10^4
Fine grids	3.54	0.001 0	560×10^4

Due to the viscous effect of the ship's bottom plate, the inlet of the duct is generally covered by the boundary layer of the ship's bottom plate. In this study, a fixed wall (with a length of 40*D*) is used to replace the ship's bottom plate in front of the duct inlet. If the length of this fixed wall is too small, it may cause the incomplete development of the boundary layer when the fluid reaches the inlet of the duct along the ship's bottom plate and ultimately affect the simulation results. Therefore, the rationality of the length of the fixed wall at the ship's bottom needs to be verified. Fig. 5 illustrates the distribution of velocities at the measuring points at different distances from the upstream boundary inlet. According to the results shown in the figure, the boundary layer can be assumed to have fully developed when the inflow reaches the measuring point 37*D* (3*D* away from the inlet of the duct), and the influence on the calculation results can thus be ignored. Therefore, the boundary length set in this study can be considered as reasonable.

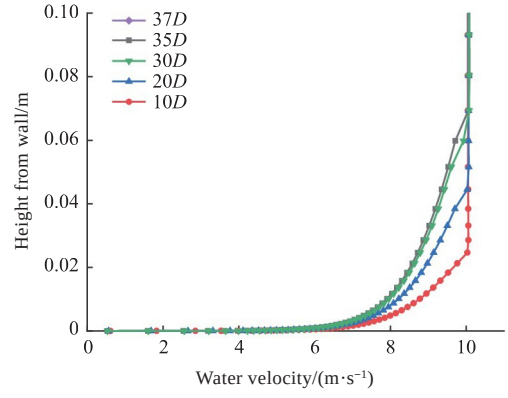

Fig. 5 Velocity profile at different measuring points on the bottom

Uncertainty analysis was performed using the Richardson extrapolation method, whose procedure is omitted here as it had been described in Reference [7]. The uncertainty calculation results of η

and ζ are shown in Table 2, in which the percentages are based on the numerical results of the fine grids. The simulation results of η exhibit oscillatory convergence, whereas those of ζ are monotonically convergent. Because the numerical solutions of η assume a state of oscillatory convergence, its uncertainty is relatively small, whereas the numerical uncertainty of ζ is relatively large. However, both uncertainties are less than 4%, which indicates that the grids in this study are well converged. The subsequent calculation will thus use the fine grids, and $y^+ \approx 5$ is obtained by referring to the grid height in Table 1.

Table 2 Uncertainty calculation results

	Grids	Numerical simulation result	Numerical uncertainty/%
η	Coarse grids	90.79	0.1
	Medium grids	90.74	
	Fine grids	90.85	
ζ	Coarse grids	0.208 8	3.9
	Medium grids	0.208 0	
	Fine grids	0.207 4	

3 Hydrodynamic performance analysis of inlet duct

The losses in the inlet duct can be divided into along-the-way loss and local loss, according to the form. In the fluid flow process, friction occurs among the liquid molecules and between those molecules and the duct, and the energy loss caused by friction overcoming is called along-the-way loss. In contrast, the drop in fluid energy due to a sharp change in the duct shape or flow direction is called local loss. The change in the inlet duct configuration would alter the duct loss. This paper focuses on the effects of different H and α on η and ζ. The variation of H (constant α) mainly affects the along-the-way loss, while the change in α (constant H) affects both the along-the-way loss and the local loss. The working conditions calculated are as follows: V_{in} = 10 m/s, Q=0.16, 0.22, 0.28, 0.35, 0.41 m^3/s, and the corresponding inlet velocity ratio *IVR* is 0.5, 0.7, 0.9, 1.1, and 1.3, respectively.

3.1 Influence of axis height on hydrodynamic performance under different working conditions

This section investigates the influence of the axis height H on the hydrodynamic performance of the duct under different working conditions. A total of five axis heights are set as H = 0.8D, 1.0D, 1.1D, 1.3D, 1.5D (D = 200 mm) and α = 33°. Fig. 6 is the surface plot of the hydrodynamic performance of the inlet duct under different axis heights (the directions of the coordinate axes are not unified for display convenience). It indicates that as *IVR*, i.e., the flow velocity in the duct rises, η first increases and then decreases slightly, and the highest efficiency point is around *IVR* = 0.9. ζ decreases rapidly as *IVR* increases, with an increasingly small decreasing amplitude. As H increases, η shows a downward trend, and a smaller *IVR* results in a slower decrease in η. An increase in efficiency is observed at *IVR* = 0.5. ζ assumes a gentle changing trend and only demonstrates a downward trend at *IVR* = 0.5. As the increase in H leads to a larger along-the-way loss, η decreases. Under the working condition of a small *IVR*, increasing H is actually equivalent to increasing the flow passage length of the duct. This is conducive to reducing the outlet flow non-uniformity, so η increases slightly.

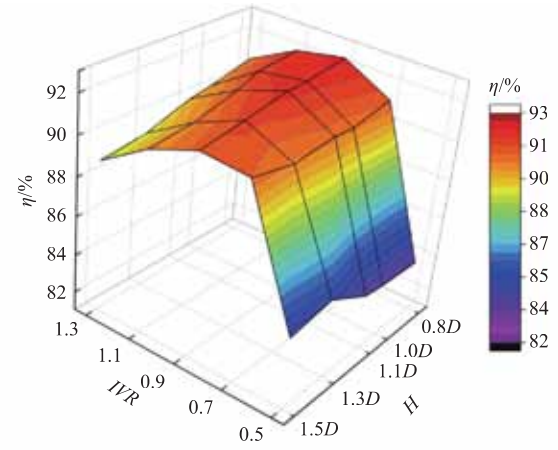

(a) Efficiency η

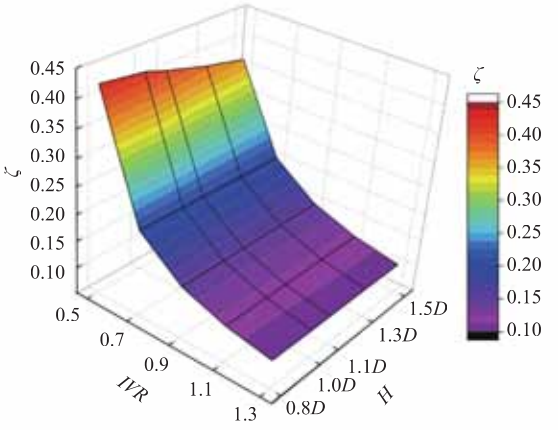

(b) Outlet flow non-uniformity ζ

Fig. 6 Hydrodynamic performance of inlet duct at different axis height H

3.2 Influence of inlet angle on hydrodynamic performance under different working conditions

This section deals with the influence of inlet angle α on the hydrodynamic performance of the duct under different working conditions. A total of four inlet angles are set as α = 21°, 27°, 33°, 39° and H = 1.0D. Fig. 7 is the surface plot of the hydrodynamic performance of the inlet duct under different inlet angles (the directions of the coordinate axes are not unified for display convenience). It demonstrates that as *IVR* increases, η first increases and then decreases, and the highest efficiency point is around *IVR* = 0.9. When α is small (α = 21°, 27°), η decreases greatly; ζ decreases rapidly with the increase in *IVR*, and the decreasing amplitude gradually shrinks. According to preliminary analysis, the reason is that as the flow velocity in the inlet duct increases, a thinner boundary layer is generated, and the proportion of the along-the-way loss caused by friction in the total energy in the duct decreases, resulting in a larger η and a more uniform outflow. However, with the further increase in flow velocity, the local loss in the duct increases relatively, and thus η decreases.

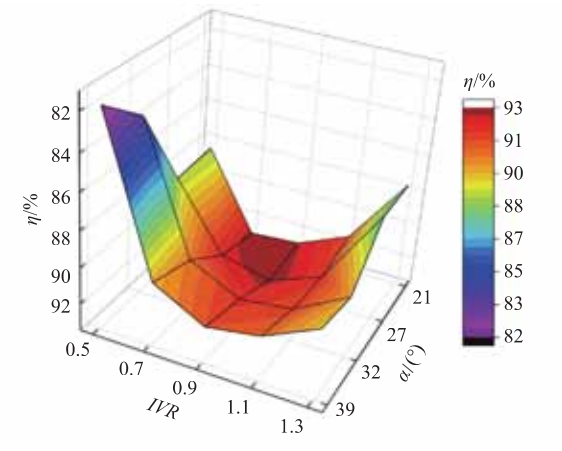

(a) Efficiency η

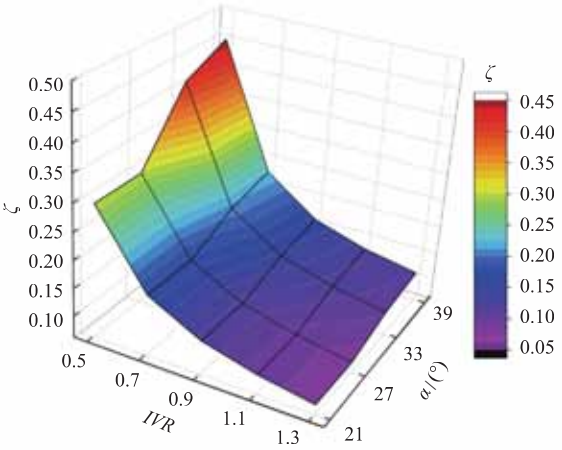

(b) Outlet flow non-uniformity ζ

Fig. 7 Hydrodynamic performance of inlet duct at different inlet angles

With the increase in α, η shows a downward trend, and a larger *IVR* causes a slower decrease in η. However, when *IVR*=1.3, η increases. In contrast, ζ demonstrates an upward trend, and a smaller *IVR* results in a faster increase in ζ. This is because the local loss increases with α. As a result, ζ rises, which leads to a decrease in η. Under the working condition of a high *IVR*, however, the upward component of the fluid is large, and a larger α is beneficial to the inflow in this case, so η increases slightly.

3.3 Flow field analysis of inlet duct

Three inlet ducts, with H = 1.0D and α = 27°, H = 1.0D and α = 33°, H = 1.3D and α = 33° respectively, were selected for flow field analysis. Fig. 8–Fig. 10 are the streamline patterns and pressure contours at the middle section of the inlet duct under different *IVR*. Illustrating the distribution of velocities at the outlet cross-section of the inlet duct (from left to right , *IVR* = 0.5, 0.7, 1.1, and 1.3, respectively), Fig. 11 reflects the outlet flow non-uniformity more distinctly. In Fig. 11, u/V_{out}-1 is the non-uniformity of axial velocities at the outlet cross-section of the duct, indicating that the figure should be now regarded as contours. A u/V_{out}-1 value closer to 0 means a more uniform axial flow. In contrast, v/V_{out} is the non-uniformity of the velocities at the outlet cross-section of the duct, meaning that the figure should now be perceived as a vectorgraph. A smaller v/V_{out} indicates more uniform flow, and v is a velocity vector at the cross-section. Fig. 8 shows that the upward velocity component of the fluid increases with *IVR*, resulting in the downward movement of the stagnation point at the lip. Therefore, when the inlet angle α is small, flow separation is highly likely to occur at the lip, resulting in a low-pressure area above the lip. In severe cases, cavitation may also occur. A comparison between Fig. 8(d) and Fig. 9(d) indicates that increasing the inlet angle α can alleviate the flow separation at the lip under a high *IVR*. Under a low *IVR* (Fig. 9(a)), however, flow separation occurs at the back of the inlet duct, leading to a larger outlet flow non-uniformity. This is also reflected in Fig. 11(b). In this case, increasing the axis height H of the inlet duct properly can reduce the flow separation at the back to a certain extent and ultimately reduce the outlet flow non-

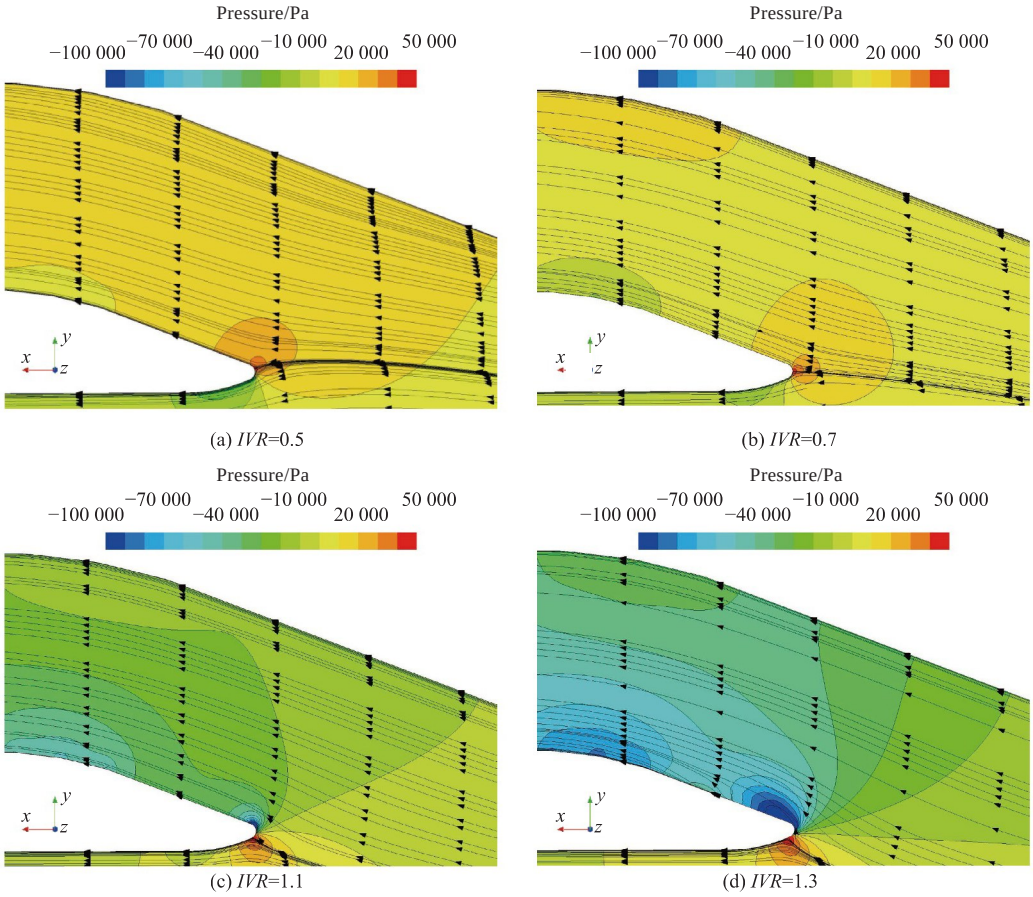

(a) *IVR*=0.5 (b) *IVR*=0.7

(c) *IVR*=1.1 (d) *IVR*=1.3

Fig. 8 Streamlines and pressure contours at middle section of inlet duct (H = 1.0D, α = 27°)

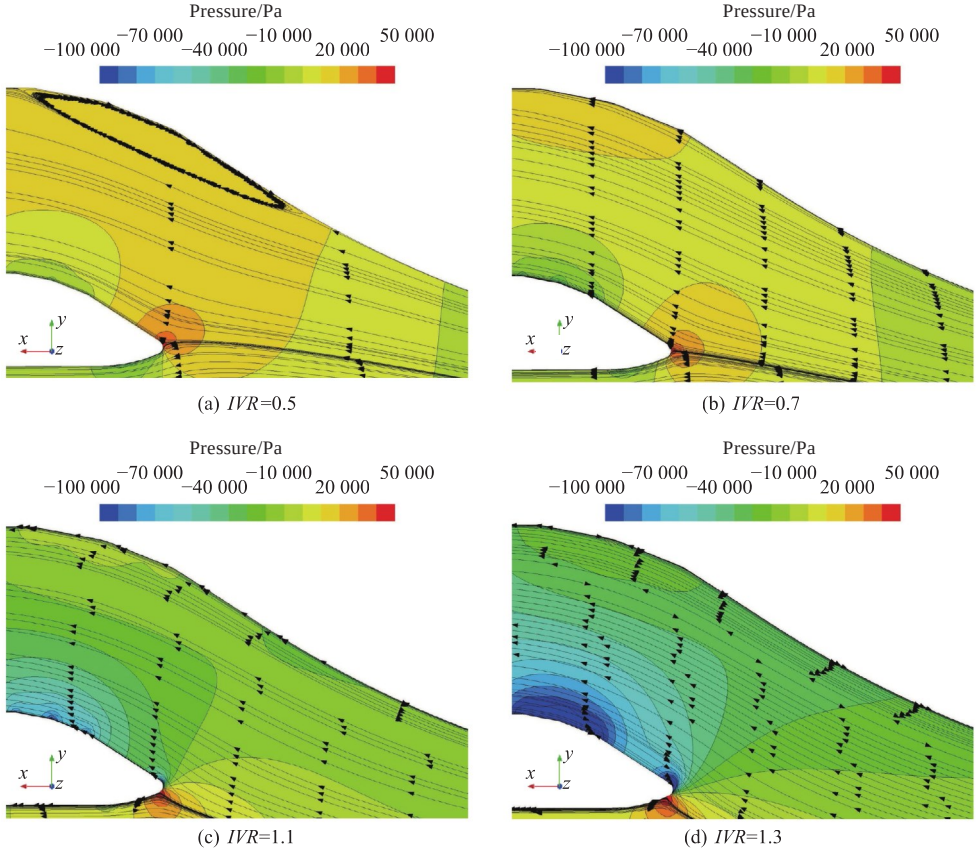

(a) *IVR*=0.5 (b) *IVR*=0.7

(c) *IVR*=1.1 (d) *IVR*=1.3

Fig. 9 Streamlines and pressure contours at middle section of inlet duct (H = 1.0D, α = 33°)

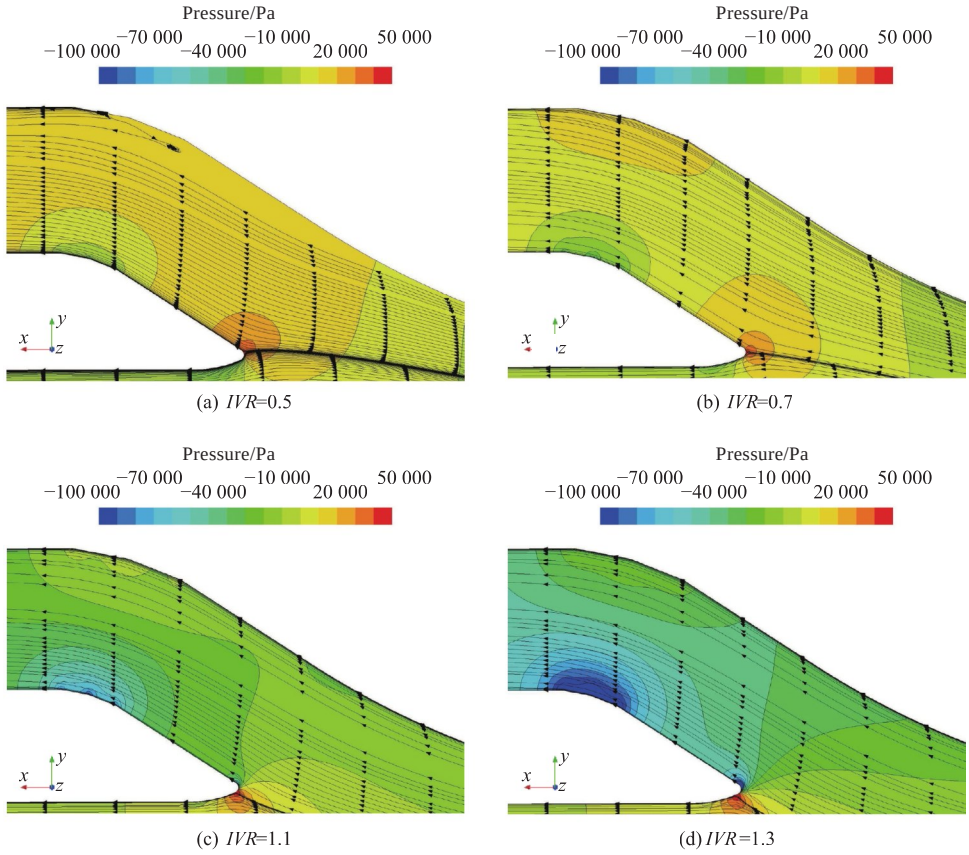

(a) *IVR*=0.5 (b) *IVR*=0.7

(c) *IVR*=1.1 (d) *IVR*=1.3

Fig. 10 Streamlines and pressure contours at middle section of inlet duct (H = 1.3D, α = 33°)

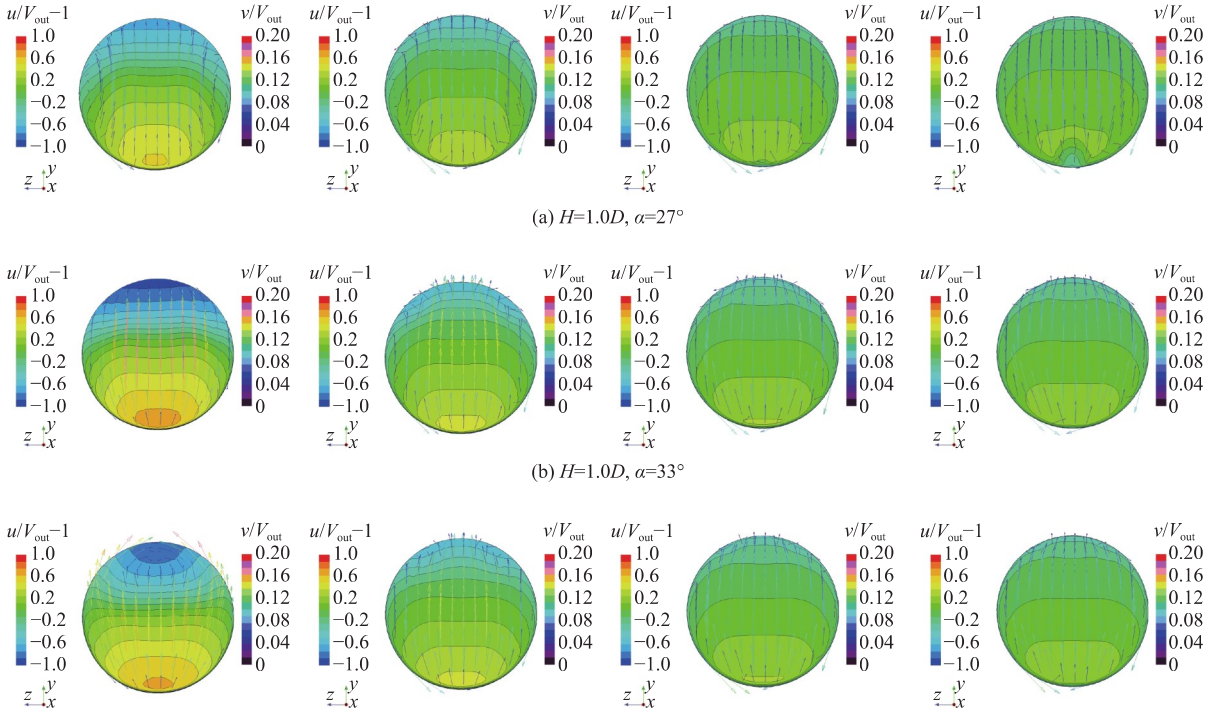

(a) H=1.0D, α=27°

(b) H=1.0D, α=33°

(c) H=1.3D, α=33°

Fig. 11 Velocity distribution at the outlet cross-section of inlet duct

uniformity (Fig. 10(a)). This conclusion can also be drawn by comparing the first figure of Fig. 11(b) with that of Fig. 11(c).

4 Conclusions

In this paper, the influences of inlet velocity ratio *IVR*, axis height H, and inlet angle α on the efficiency of the inlet duct and the outlet flow non-uniformity are respectively analyzed by CFD numerical simulation. The numerical values of the above model under different *IVR* (0.5−1.3) were simulated by setting five H and one α and one H

and four α respectively.

Regarding hydrodynamic performance, the efficiency of the inlet duct is high when *IVR* = 0.7−1.1, and the corresponding loss is small. In the high-efficiency range (*IVR* = 0.7−1.1), setting a too large *H* and α is not conducive to the efficiency and the outlet flow non-uniformity. In fact, when ship speed and main engine power are set, the operating status of the pump can be determined according to the *IVR* selected. According to the flow field characteristics, increasing α can reduce the flow separation at the lip under a high *IVR*, and increasing *H* can alleviate the flow separation at the back under a small *IVR*. Nevertheless, *H* and α are often restricted by the layout space. In summary, during the design of the inlet duct parameters, the key parameters should be weighed and selected in the high-efficiency range according to the working conditions after the matching of the ship and pump.

References

[1] ZHANG Z, WANG L X. Estimation for inlet boundary layer effect coefficient around waterjet duct [J]. Ship & Boat, 2008, 19 (3): 10−14 (in Chinese).

[2] QIAN H, SONG K W, GUO C Y, et al. Influence of waterjet duct on ship's resistance performance [J]. Chinese Journal of Ship Research, 2017, 12 (2): 22−29 (in Chinese).

[3] SHI J, FENG X D, LI G C, et al. Influence of the inlet length upon hydrodynamics performance for ship's water jet propulsion [J]. Ship & Ocean Engineering, 2016, 45 (6): 81−84, 88 (in Chinese).

[4] LI C, SHU X H, ZHAO C S. Research on the influence of waterjet duct performance based on inclination of waterjet duct [J]. Ship Science and Technology, 2017, 39 (9): 49−53 (in Chinese).

[5] JI G R, CAI Y L, LI N, et al. Influence of lip parameters on non-uniformity and stagnation point at inlet duct of waterjet propulsion [J]. Shipbuilding of China, 2016, 57 (4): 109−115 (in Chinese).

[6] YANG F Q, WANG X Z, JIANG J W, et al. Parametric analysis of the inlet duct in the marine waterjet propulsor [J]. Journal of Mechanical & Electrical Engineering, 2109, 36 (11): 1212−1215 (in Chinese).

[7] ITTC. Uncertainty analysis in CFD, verification and validation methodology and procedures: 7.5-03-01-01 [R]. ITTC-Recommended Procedures and Guidelines, 2021.

[8] ITTC. Uncertainty analysis in CFD, examples for resistance and flow: 7.5-03-02-01 [R]. ITTC-Recommended Procedures and Guidelines, 1999.

[9] ITTC. The specialist committee on validation of waterjet test procedures, final report and recommendations to the 24th ITTC [R]. Proceedings of the 24th ITTC, 2005.

喷水推进器进口流道水动力性能分析

邱继涛[*1,2], 尹晓辉[1,2], 王仁智[2]

1 喷水推进技术重点实验室,上海 200011

2 中国船舶及海洋工程设计研究院,上海 200011

摘　要:[**目的**]研究喷水推进器进口流道主参数对其性能的影响,为喷水推进器设计提供依据。[**方法**]基于STAR-CCM+商业软件,通过定常雷诺平均NS方程(RANS),数值模拟分析不同进速比(*IVR*)工况下喷水推进器进口流道轴线高度和进流角度对其水动力性能的影响,并根据国际拖曳水池会议(ITTC)的不确定度分析规程进行数值不确定度分析。采用六面体结构化网格对计算域进行离散,采用Realizable k-ε 两层湍流模型对控制方程进行封闭,离散格式为二阶。压力—速度耦合计算选用压力耦合方程组的半隐式算法(SIMPLE)。[**结果**]结果显示,数值的不确定度小于4%,表明所采用的网格收敛性良好,数值结果可靠。[**结论**]研究表明,当*IVR* =0.7~1.1时,进口流道效率较高;对于*IVR*较大的工况,应减小进流角;对于*IVR*较小的工况,则应适当增加轴线高度,以改善出口流动的不均匀度。

关键词:喷水推进器;进口流道;数值不确定度;水动力性能